Numerical Investigation of Aerodynamic Performance and Loads of a Novel Dual Rotor Wind Turbine

Behnam Moghadassian*, Aaron Rosenberg†, Hui Hu‡, and Anupam Sharma§

Department of Aerospace Engineering,

Iowa State University, Ames, IA, 50011.

The objective of this paper is to numerically investigate the effect of the atmospheric boundary layer on the aerodynamic performance and loads of the novel dual-rotor wind turbine (DRWT) proposed by Rosenberg *et al.*[1] Assuming that the turbine operates in isolation, numerical analyses are carried out for two atmospheric stability conditions: (1) neutral, and (2) stable. Comparisons are drawn with the corresponding analyses of a comparable conventional single-rotor wind turbine (SRWT) to assess changes in: (a) aerodynamic efficiency, and (b) dynamic loads on the turbines. The results show that the DRWT improves isolated turbine performance even when atmospheric boundary layer effects are considered. It is also found that the DRWT enhances wake mixing when background turbulence due to the atmospheric boundary layer is moderately high. This has implications on wind plant performance when multiple turbines are placed one behind the other.

No significant increase in aerodynamic loads is observed in the DRWT design. In fact, the out-of-plane blade root moment of the main rotor is reduced in the DRWT. Spectral analyses show peaks in unsteady loads at the rotor blade passing frequency and its harmonics for both the primary and secondary rotors. Loads at other (combination) frequencies are observed in the secondary rotor.

I. Introduction and Background

The maximum theoretical power coefficient of a horizontal axis wind turbine (HAWT) was derived by Betz to be 59.3%. However, simplifications made in Betz' 1D control volume analysis as well as other constraints in HAWT design result in a more practical limit of around 50%. Since the levelized cost of energy (LCOE) is inversely proportional to the power coefficient (C_P), there has been significant effort towards increasing C_P. One method of increasing C_P involves adding additional rotors to a conventional HAWT. Wind turbines with two rotors (typically arranged in tandem so that the incoming flow stream area is unchanged) are known as dual rotor wind turbines (DRWT).

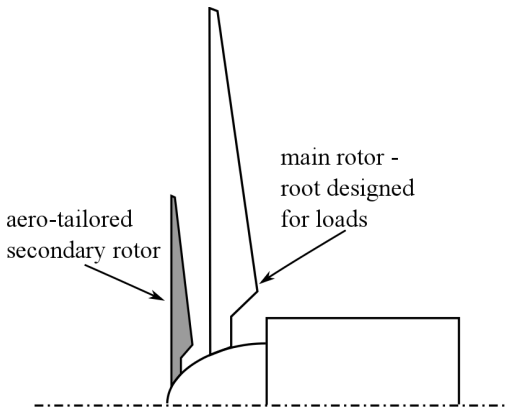

Figure 1: A cartoon of the DRWT technology by Rosenberg *et al.*[1]

There have been a few efforts at improving turbine C_P using the DRWT approach. Jung *et al.*[2] explores a 30 kW counter-rotating wind turbine installed in Korea. It features an 11 meter diameter main rotor with a 5.5 meter auxiliary rotor located upwind of the main rotor. This DRWT uses a bevel gear to couple the counter-rotating shafts. The authors use quasi-steady strip theory and a wake model to predict the performance of several DRWT configurations. They predicted a 9% increase in power coefficient when compared with a single-rotor configuration. Several studies have led to patents including Kanemoto

*Ph.D. student, Aerospace Engineering, 1200 Howe Hall, Ames, IA, 50011, and AIAA Student Member

†Ph.D. student, Aerospace Engineering, 1200 Howe Hall, Ames, IA, 50011, and AIAA Student Member

‡Professor, 2251 Howe Hall, Aerospace Engineering, Ames, IA, 50011, and AIAA senior member

§Assistant Professor, 2341 Howe Hall, Aerospace Engineering, Ames, IA, 50011, and AIAA senior member

and Galal[3,4] who propose a DRWT with two different sized upwind rotors driving a generator with two rotating armatures.

The DRWT technology by Rosenberg *et al.*[1] (see Fig. 1) takes a different approach - it aims at reducing losses rather than increasing energy capture through increased rotor area (from the secondary rotor). It utilizes a secondary, smaller, co-axial rotor to mitigate root losses and to enhance mixing of the turbine wake. Rosenberg *et al.*[1] and Selvaraj[5] introduced this turbine technology and presented preliminary aerodynamic analyses of a DRWT design. The conceptual 5 MW offshore turbine by NREL[6] was used as the baseline single-rotor design and also as the main rotor for the DRWT. The secondary rotor was designed using an inverse design approach based on the blade element momentum theory. The design and optimization approach used Reynolds Averaged Navier-Stokes (RANS) computational fluid dynamics (CFD) simulations with an actuator disk representation[7] of turbine rotors. For the optimization analyses, axisymmetric flow assumption was employed to dramatically reduce the computational cost. RANS CFD analyses showed an increase in turbine power coefficient (C_P) of around 7% with the DRWT. Figure 2 shows selected RANS optimization results from Ref. 1. Preliminary investigations of turbine wake evolution were also conducted by performing LES simulations for isolated turbines in uniform flow with no atmospheric (inflow) turbulence. While the LES results corroborated the RANS findings in isolated turbine C_P increase, no significant increase in wake mixing was observed. The absence of atmospheric turbulence was identified as a potential reason for the imperceptible change in wake mixing.

In this paper, we extend the analyses of Refs. 1 and 5 by including the effect of atmospheric boundary layer. We present comparative (between DRWT and SRWT) isolated turbine aerodynamic analyses for two atmospheric stability conditions - neutral and stable. One of the concerns with the DRWT technology is the potentially increased unsteady loads on the main turbine due to the proximity of the main and secondary rotors. Numerical analyses performed to compute these loads are reported as power spectral densities of blade root moments (out-of-plane components) and axial (thrust) force.

The remainder of the paper is laid out as follows. A summary of the numerical method utilized in this study and its validation against experimental data are presented first. A short section then summarizes the setup, grids, and simulation details including the assumptions made for the present calculations. Aerodynamic performance results are described next wherein comparisons between SRWT and DRWT for neutral and stable atmospheric conditions are drawn. The following section then reports the aerodynamic loads on the two rotors of the DRWT for the two atmospheric stability conditions considered. The conclusions from this investigation are presented at the end.

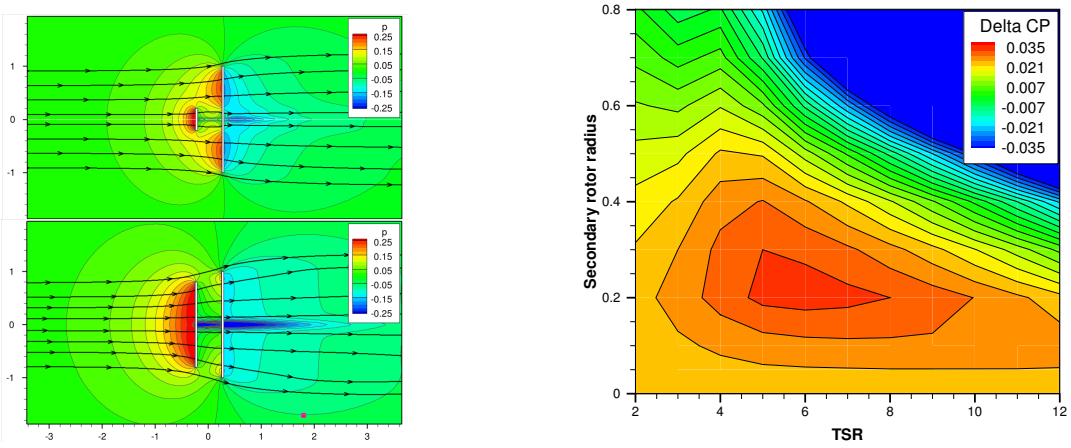

(a) Simulations for two rotor sizes

(b) ΔC_P (DRWT - SRWT)

Figure 2: RANS simulation results reproduced from Ref. 1: (a) parametric study varying secondary rotor radius, and (b) difference in aerodynamic power coefficient, $\Delta C_P = C_{P\text{DRWT}} - C_{P\text{SRWT}}$ due to the addition of the secondary rotor.

II. Numerical Methods

Wind turbine and wind plant aerodynamics can be modeled with a spectrum of tools that vary considerably in fidelity and computational complexity (cost). Analytical[8,9] and semi-analytical models,[10] parabolic wake models,[11] Reynolds Averaged Navier-Stokes (RANS) simulations,[12] and Large Eddy Simulations (LES), all play different, yet necessary roles in turbine/plant analysis and design. Vermeer[13] and Sanderse[14] provide excellent reviews of various numerical methods available to study wind turbine and wind plant aerodynamics.

Modeling wind turbine and wind plant aerodynamics using LES has received a lot of research attention in recent years (see e.g., Refs. 15–19). Jimenez *et al.*[17,18] used incompressible LES to model a single wind turbine (modeled as an actuator disk) aerodynamics in an atmospheric boundary layer. Modest agreement of their predictions with field-measured Reynolds stresses was observed. Troldborg *et al.*[19] investigated aerodynamic interaction between two turbines using an actuator line model coupled with their LES solver, EllipSys3D. The desired velocity shear (corresponding to neutral atmospheric stability) and turbulence was obtained by applying body forces in the entire domain. Aerodynamic interaction between the turbines was simulated for varying atmospheric turbulence intensity, distance between the turbines, and partial and full-wake operation of the downstream turbine.

The Simulator fOr Wind Farm Application (SOWFA)[20,21] software is used here. In this LES model, spatially filtered, incompressible forms of continuity and Navier-Stokes equations are solved using spatial and temporal discretization. Spatial filtering introduces unresolved, sub-filter scale (also called sub-grid scale or SGS) stresses, which have to be modeled. The width of the spatial filter is taken to be the grid-filter width given by $\Delta = (\Delta_x \Delta_y \Delta_z)^{1/3}$. The actuator line model (ALM) is used for rotor parameterization. Denoting spatially-filtered quantities by $\widetilde{(\,)}$, the governing fluid flow equations are

$$
\begin{aligned}
\frac{\partial \widetilde{u_i}}{\partial x_i} &= 0, \\
\frac{\partial \widetilde{u_i}}{\partial t} + \widetilde{u_j}\left(\frac{\partial \widetilde{u_i}}{\partial x_j} - \frac{\partial \widetilde{u_j}}{\partial x_i}\right) &= -\frac{\partial \widetilde{p^*}}{\partial x_i} - \frac{\partial \tau_{ij}}{\partial x_j} + \nu \frac{\partial^2 \widetilde{u_i}}{\partial x_j^2} \\
&- \underbrace{f_i/\rho_0}_{\text{turbine force}} + \underbrace{\delta_{i1} F_P}_{\text{driving pressure}} + \underbrace{\delta_{i3} g_0 (\widetilde{\theta} - \langle \widetilde{\theta} \rangle)/\theta_0}_{\text{buoyancy force}} + \underbrace{F_c \epsilon_{ij3} \widetilde{u_j}}_{\text{coriolis force}}, \\
\frac{\partial \widetilde{\theta}}{\partial t} + \widetilde{u_j} \frac{\partial \widetilde{\theta}}{\partial x_j} &= -\frac{\partial q_j}{\partial x_j} + \alpha \frac{\partial^2 \widetilde{\theta}}{\partial x_j^2},
\end{aligned}
$$

where, $\widetilde{p^*} = \widetilde{p}/\rho_0 + \widetilde{u_i}\widetilde{u_j}/2$ is the modified kinematic pressure, $\tau_{ij} = \widetilde{u_i u_j} - \widetilde{u_i}\widetilde{u_j}$, is sub-grid scale (SGS) stress tensor, and $q_j = \widetilde{u_j \theta} - \widetilde{u_j}\widetilde{\theta}$ is SGS heat flux. f_i is momentum source to model forces exerted by turbine blades, $\delta_{i1} F_P$ is pressure gradient to drive flow, θ is potential temperature and α is thermal diffusivity of the fluid. The deviatoric part of the SGS stress tensor, τ_{ij} is typically modeled using an eddy-viscosity model, $\tau_{ij} - 1/3\ \delta_{ij}\tau_{kk} = -2\nu_{sgs}\widetilde{S_{ij}}$ and the SGS heat flux with an eddy-diffusivity model $q_j = \widetilde{u_j \theta} - \widetilde{u_j}\widetilde{\theta} = -(\nu_{sgs}/Pr_{sgs})\partial\widetilde{\theta}/\partial x_j$, where, $\widetilde{S_{ij}} = 1/2\ (\partial \widetilde{u_i}/\partial x_j + \partial \widetilde{u_j}/\partial x_i)$ is the resolved strain-rate tensor and Pr_{sgs} is the SGS Prandtl number. The mixing-length model by Smagorinsky,[22] $\nu_{sgs} = (C_S \Delta)^2 |\widetilde{S}|$ is used to model ν_{sgs}. In the original model, C_S was assumed to be a constant, but dynamic calculation of this coefficient has been used in recent years. Improved, tuning-free, scale-dependent SGS models have also been developed (see e.g., Ref. 15) and used for atmospheric flow and wind plant simulations.

SOWFA uses a finite volume formulation and the discretization is second order accurate in space (central) and time (backward). A two-step solution procedure is used. In the first (precursor) step, the turbines are removed and turbulent flow in the domain is calculated. After the solution reaches a quasi-equilibrium state, time-accurate data is sampled at every time step on the "inlet" plane and stored. This data is specified as a boundary condition for the subsequent wind plant calculations. Other researchers[16,23] have used periodic BCs with a buffer layer where the mean velocity is scaled to the desired vertical profile.

Viscous effects are negligible everywhere except near surfaces due to high Reynolds number. Energy containing eddies near the ground can become very small, and resolving such small scales will lead to exorbitant grid sizes. Surface flux models for stress and heat (e.g., the models by Moeng[24]) are therefore usually used in wind plant computations. Moeng's models require as input the surface roughness height, h_0, the horizontally-averaged surface heat flux, q_s, and a measure of the horizontally-averaged shear stress specified as friction velocity, u_*. While h_0 and q_s are directly specified (from estimates in literature for

different surfaces - sea, grasslands, forest, etc.), u_* is approximated using the Monin-Obhukhov similarity theory.[25]

Lee *et al.*[26] coupled the LES solver for wind plant aerodynamics, SOWFA with the structural dynamics solver in the FAST (Fatigue, Aerodynamics, Structures, and Turbulence) code[27] to enable calculation of fatigue loads due to atmospheric and wake turbulence. Through this coupling, the simplified aerodynamics module (including the turbulent inflow model) in FAST is replaced by LES, which provides much higher fidelity in resolving the flow, although the structural dynamics model is arguably relatively too simple. Since the focus of this paper is limited to aerodynamic performance and loads, and not aeroelasiticity, we idealize our turbine by assuming the rotor blades to be infinitely stiff. The other structures e.g., the tower and the nacelle, are not modeled in these simulations. We further assume that the turbine operates at a fixed rotation rate regardless of the incoming flow velocity, which varies with time because of the atmospheric turbulence.

A. Code Scalability

Large eddy simulations of wind turbine/plant aerodynamics with adequate spatial and temporal resolution require large amounts of memory as well as compute time. Parallel computing is used to obtain results in reasonable time on large computational meshes that resolve the relevant flow physics. In order to make efficient use of the parallel computing resources, a scaling study was performed on the Stampede computer cluster. The Stampede cluster consists of 6400 compute nodes, each node fitted with two Intel Xeon E5-2680 processors and one Intel Xeon Phi SE10P Co-processor, and with 32 GB of memory. The E5-2680 is a 64 bit processor with 8 cores and has a clock speed of 2.7 GHz. This supercomputer is maintained and operated by the Texas Advanced Computing Center (TACC) at the University of Texas at Austin.

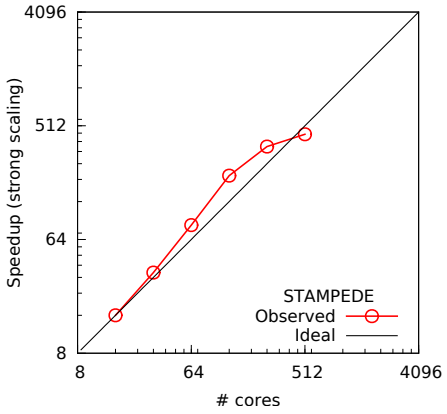

Figure 3: Scaling study using SOWFA on the Stampede computer cluster.

Figure 3 plots the results from the scaling study. The study was conducted with a fixed computational size (mesh), hence the results represent "strong" scaling of the solver. Super-linear speedup is observed between 16 to 256 cores. Increasing number of cores beyond 512 resulted in a penalty. The parallel simulations were therefore carried out on anywhere between 128–512 cores per run.

III. Computational Setup

We use a two-step simulation approach where the atmospheric boundary layer flow is computed first on one grid and then the flow around the wind turbine is computed on another, more refined grid. Two atmospheric boundary layer (ABL) conditions are considered: (1) neutral ABL, and (2) stable ABL. In our simulations, the wind blows from the west boundary (inlet) to the east boundary (outlet). We simulate 600 seconds of turbine operation for each ABL condition.

The turbulence in the atmospheric boundary layer is developed in the computational domain by performing "precursor" simulations. A precursor calculation simulates an infinitely long domain (the Earth surface) using cyclic boundary conditions in all directions except the top and the bottom boundaries. There is no wind turbine inside the computational domain in the precursor runs. The flow is driven by a pressure gradient which is adjusted to achieve the desired flow speed at the hub height. This simulation is carried out for a long enough time to achieve a statistically stationary turbulent flow state. In our simulations, it takes approximately 12000 seconds to reach statistical stationarity. The entire flow field at this time instant is stored to initialize the wind turbine/plant calculation.

Data sampling at the inlet boundary is initiated after reaching statistical stationarity (around $t = 12000$ s) to collect time-accurate data. This time-accurate data, stored as primitive flow variables, is prescribed as inflow conditions in the wind turbine/plant simulations. Another 600 seconds of atmospheric flow simulation is carried out to "bank" sufficient data at the inlet boundary. The need to collect inflow data arises from the fact that periodic (cyclic) boundary conditions cannot be used in the streamwise direction in wind

turbine/plant aerodynamics simulations, which are typically carried out on a finite (reasonably sized) domain. The presence of strong wakes downstream of the turbines significantly changes the flow between the inlet and outlet boundaries as explained in Witha *et al.*[28] To avoid the exorbitant computational cost associated with resolving to the wall, wall models by Moeng[24] are used to estimate the surface stresses (viscous and SGS) and temperature flux at the wall (Bottom) boundary. A zero-pressure gradient boundary condition is used on the Top boundary of the domain to allow for non-zero mass, momentum, and energy flux. Periodic boundary conditions are still used on the North and South boundaries. The inlet is on the West boundary and a zero-pressure gradient boundary condition to simulate outlet conditions is applied on the East boundary.

The wind turbine simulation starts at $t = 12000$ seconds. The initial flow field in the computational domain is interpolated from the stored data (at $t = 12000$ s) of the precursor simulation. At each time step the velocity and temperature at the inlet boundary are mapped from the boundary data stored during the precursor simulation. Turbulent inflow is thus prescribed during the entire wind turbine simulation.

The computational domains for the precursor ABL and the wind turbine simulations need not be identical. In fact, it is desirable to make the precursor ABL domain large and the wind turbine domain short. This is in accordance with the length scale disparity between the two simulations. In the precursor ABL simulation, the energy containing length is are of the order of a kilometer (planetary boundary layer height). In the wind turbine simulation however, our interest is also in capturing the turbulence in the turbine wake, where the dominant length scale is of the order of the turbine diameter ($\approx$ 100 m). A shorter domain allows for greater spatial resolution. As can be seen in Fig. 4, the precursor runs are performed on a computational domain with dimensions $8D \times 8D \times 8D$, where D=126 m. The domain is discretized into $150 \times 150 \times 200$ cells. The precursor runs are performed on 128 processors and each run takes about 9 hours of wall-clock time. The wind turbine runs are performed on a domain of size $8D \times 4D \times 4D$ that is discretized into $380 \times 100 \times 100$ cells. The turbine is placed at a distance of 2D downstream of the inlet. Only the turbine rotors are simulated; the hub and nacelle are ignored in these simulations. OpenFOAM's blockMesh utility is used to generate the computational meshes. The mesh for wind turbine simulations is refined in the axial direction near the rotor before gradually stretching downstream. It takes approximately 6.5 hours to simulate 600 seconds of flow in each wind turbine simulation using 256 processors in parallel.

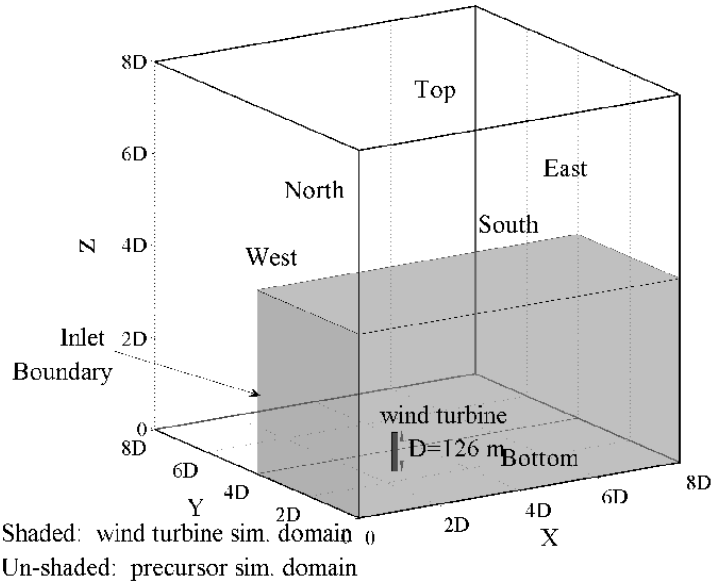

Figure 4: A schematic showing the computational domains for the atmospheric boundary layer (precursor) and the main (wind turbine) simulations.

LES simulations are carried out using the optimum DRWT identified in Rosenberg *et al.*[1] The non-dimensional chord and twist distributions of the main rotor and the secondary rotor of the DRWT are shown in Fig. 5. Note that the blade chord (c) and radius (r) are non-dimensionalized by the respective rotor tip radius, i.e., the secondary rotor is normalized using the secondary rotor tip radius, while the primary rotor values are normalized using the primary rotor tip radius. To enable direct comparisons, simulations are also performed for conventional single rotor wind turbine (SRWT), which is the conceptual NREL 5MW offshore reference turbine.[6]

IV. Results and Discussion

The objectives of the DRWT design proposed by Rosenberg *et al.*[1] are twofold: (1) minimize root losses, and (2) increase entrainment from the upper atmosphere into the turbine wake. An increase in C_P of between

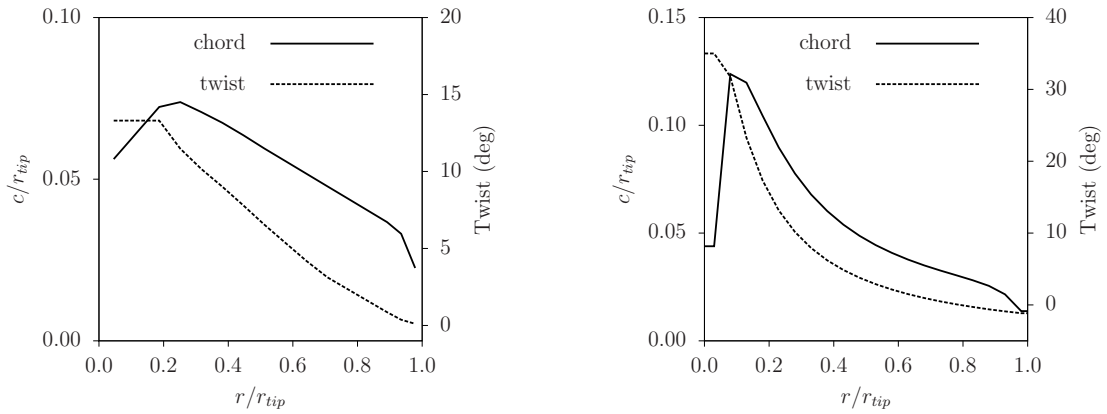

(a) Primary rotor (b) Secondary rotor

Figure 5: Radial distributions of the (a) primary and (b) secondary rotor blade chord and twist.

5-7% through root loss mitigation was already demonstrated for uniform inflow calculations in Rosenberg *et al.*[1] Here we analyze the effect of atmospheric boundary layer on both root losses and entrainment.

A. Atmospheric Boundary Layer

We first analyze the atmospheric boundary layer (ABL) simulations. The simulated flow data is averaged in time and space to obtain mean velocity profiles for both the neutral and stable ABL conditions. A pressure gradient along the flow direction is imposed and is continually adjusted until the desired mean flow speed (9 m/s for the simulations here) is achieved at hub height. The atmospheric stability is varied by changing the heat flux through the bottom boundary. A large negative value (indicating heat leaving the computational domain) is specified to simulate the stable ABL condition, while no net heat flux is applied for the neutral ABL simulation. Figure 6 plots the velocity profiles for the two ABL cases studied. The vertical shear in wind speed near the ground in the stable case is much higher than in the neutral case as expected.

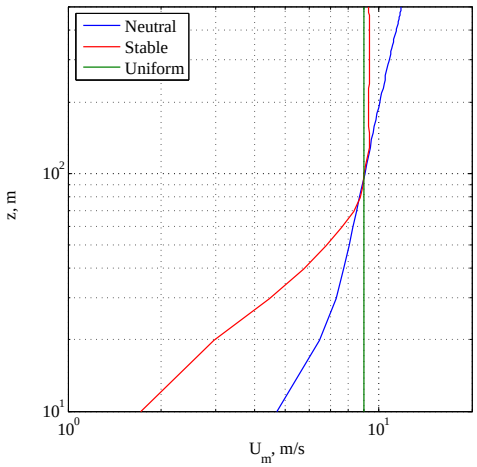

Figure 6: Velocity profiles for the two ABL conditions simulated: neutral and stable.

Atmospheric boundary layer profile is often characterized using the power law in the form of $u(z) = u_{ref}(z/z_{ref})^{\alpha}$. The velocity profiles in Fig. 6 are fitted into the above power law formula to compute the exponent α. According to Ref. 29, u_{ref} is the wind speed at the height of 10 m and α is found using the wind speed at the height of 80 m as $\alpha = \ln(u_{80}/u_{10})/\ln(80/10)$. The values of α are found to be 0.163 and 0.597 for neutral and stable conditions respectively.

B. Aerodynamic Performance

Root Loss Mitigation

The smaller secondary rotor of the DRWT proposed by Rosenberg *et al.*[1] is intended to mitigate the losses due to the non-optimum root section (inner 25%) of the larger primary rotor. Since the root of the primary rotor is designed to withstand the high loads associated with its size, it does not effectively capture the momentum in the inner region of the streamtube. Airfoils in this region have very high thickness-to-chord ratio and thus have poor aerodynamic performance. In many cases, this region produces negative torque,

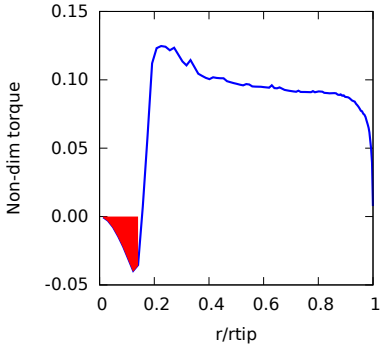

Figure 7: Spanwise variation of non-dimensional torque.

impeding the rotation of the rotor (see Fig. 7). Aerodynamic losses due to poor root aerodynamics have been shown to be on the order of 5%. The secondary rotor is added to capture the energy otherwise lost by the primary rotor.

RANS calculations by Rosenberg *et al.*[1] show an increase in power coefficient of 7% with the addition of the second rotor. Here we have corroborated these results using LES for the three different atmospheric conditions identified in Section III. The DRWT outperforms the conventional SRWT in all three conditions. In the uniform flow, the DRWT generates 4.9% more power than the SRWT. It generates 5.2% and 10.8% more power in the stable and neutral simulations respectively.

Turbine Wake Mixing

Comparative wake mixing analyses are performed for the DRWT and SRWT configurations in two different atmospheric stability conditions. Figure 8 compares the circumferentially averaged, normalized mean velocity ($\langle \bar{u}/u_\infty \rangle$) profiles along the rotor radius in the wake region. The angle brackets here denote spatial (azimuthal) averaging, while the overbar denotes time averaging. Time averaging is performed over 90 rotor revolutions. It should be noted that atmospheric turbulence can contain energy at frequencies much lower than blade passing frequency (associated with large scale eddies), hence averaging over much larger time, as performed here, is required.

Comparisons are drawn at four locations downstream of the turbine: $0D$, $2D$, $4D$, & $6D$, where D is the main rotor diameter. The location $0D$ is taken immediately downstream of the turbine. Reduced values of $\langle \bar{u}/u_\infty \rangle$ are observed in the wake of the DRWT as compared to SRWT for $r/r_{tip} < 0.4$ for $x < 4D$ due to more efficient extraction of energy by the secondary rotor of the DRWT. For the neutral stability case, the mean wake velocity near the tip region shows faster recovery for the DRWT than the SRWT in the first few diameters. Further downstream (around $6D$) however, the difference in wake velocities between the two turbines is small, with the DRWT showing higher recovery than SRWT.

In the stable case, the wake recovery is less than the neutral case due to the reduced background turbulence in the atmospheric boundary layer. In this case, the default operation of the DRWT does not seem to enhance wake mixing near the tip region. However, the difference in velocity deficit between the DRWT and SRWT in the wake near the hub height is substantially reduced $6D$ downstream of the turbine. This suggests that in low atmospheric turbulence, even though the *de facto* operation of the DRWT does not enhance wake mixing near the tip, the wake deficit due to the secondary rotor is sufficiently mixed out that it will not adversely impact the performance of downstream turbines if they are placed at least $6D$ apart.

Since mechanical turbulence (due to velocity shear) is the primary mechanism of wake mixing, turbulence intensities in turbine wakes are compared between the DRWT and SRWT configurations in Fig. 9. In general, the turbulence intensities for the DRWT are higher for both neutral and stable ABL conditions. Higher turbulence intensities explain the higher wake mixing seen for the DRWT.

Momentum Entrainment

In most wind plants, turbines are installed in a systematic arrangement (array). Wake losses in such turbine arrays are most severe when the wind direction is perfectly aligned with the turbine rows or columns. In such extreme cases, it is meaningful to look into entrainment of high-momentum fluid into the turbine wake layer. Of particular interest then is the momentum flux through a hypothetical cylinder located directly downstream of a wind turbine (see Fig. 10). This cylinder has the same radius as the main rotor ($r_{tip} = 63$) and it extends from $2D$ upstream to $6D$ downstream of the rotor. Its axis is aligned with the rotor axis. Time-averaged velocity data, including the Reynolds stress tensor, is interpolated onto this cylinder from the simulations using Tecplot.

Entrainment of high momentum fluid into this cylinder is induced by turbulent stresses, particularly the stress term $\overline{u'_r u'_x}$, where the subscript 'r' denotes the radial component, the superscript $(\,)'$ denotes a perturbation quantity, and the overline denotes a time-averaged quantity. To get the cumulative effect of entrainment (from all around the cylinder), this component of the stress tensor ($\overline{u'_r u'_x}$) is further averaged azimuthally. This spatial averaging procedure is denoted by angle brackets; thus the quantity $\langle \overline{u'_r u'_x} \rangle$ represents temporally and spatially averaged value of $u'_r u'_x$ and its magnitude signifies the flux of axial momentum through the cylinder. Figure 11 plots the variation of this averaged quantity with distance from the turbine rotor location. Variation is shown for both stable and neutral ABL conditions and is plotted on the same scale to contrast the mixing rates in between the two stability conditions tested. u'_r is taken to be positive

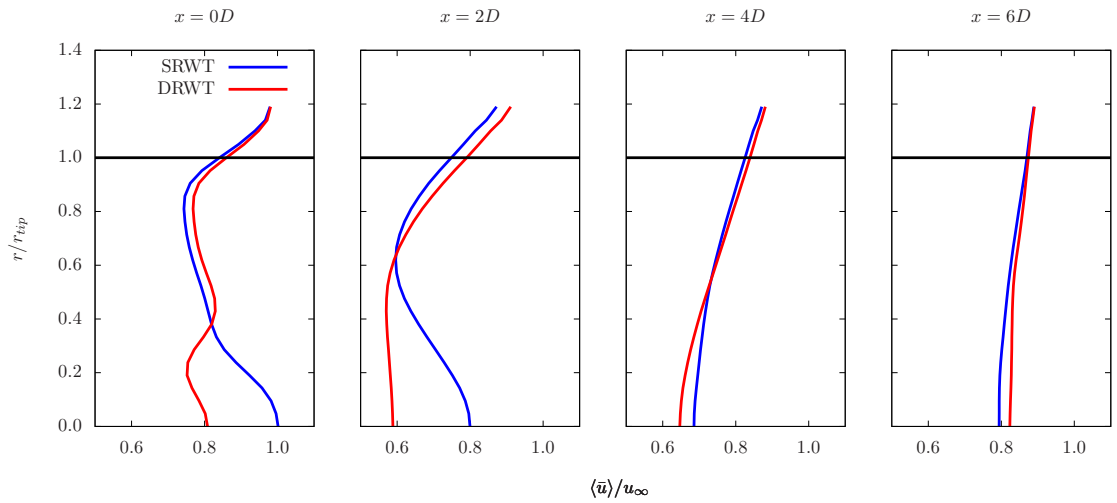

(a) Neutral

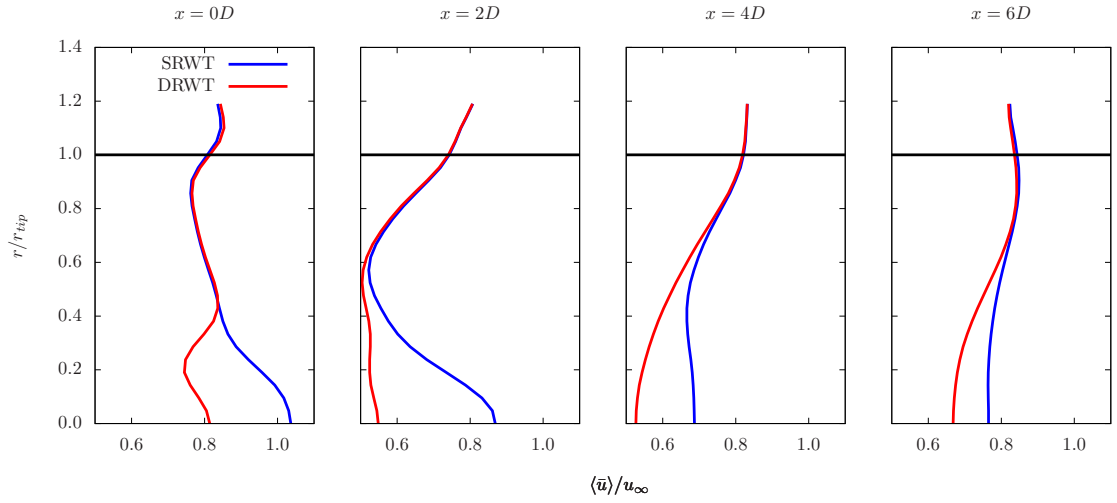

(b) Stable

Figure 8: Comparison between SRWT and DRWT of circumferentially averaged mean axial velocity at four downstream locations ($x/D = 0, 2, 4, \&6$) for (a) neutral, and (b) stable atmospheric conditions.

for outgoing velocity, therefore negative values of $\langle \overline{u'_r u'_x} \rangle$) indicate momentum flux into the cylinder. The large difference in mixing rates between the stable and neutral ABL conditions is due to the high level of turbulence in the neutral ABL.

In comparing the entrainment between the DRWT and the SRWT, it should be borne in mind that for these simulations, the secondary rotor is operated at the tip speed ratio that gives maximum aerodynamic performance for *isolated* turbine performance in uniform inflow conditions. No attempt is made here to optimize the secondary rotor operation or the geometry to enhance wake mixing or to account for the atmospheric boundary layer. Notwithstanding the sub-optimal design/operation, the DRWT still shows higher level of entrainment than the SRWT in the neutral stability condition. The difference between the two geometries is however negligible for the stable ABL simulation. The stable ABL condition has relatively too little atmospheric (background) turbulence to sufficiently stimulate mixing of the trailing blade wakes/vortices of the two rotors of the DRWT. This result is a bit unfortunate as it is primarily in stable ABL conditions that enhanced mixing is required. Nevertheless, the fact that the turbine operation, and possibly the geometry of the secondary rotor, can be optimized to actively target wake mixing, leaves a potential for improvement yet to be gained from the DRWT concept in terms of wind plant performance.

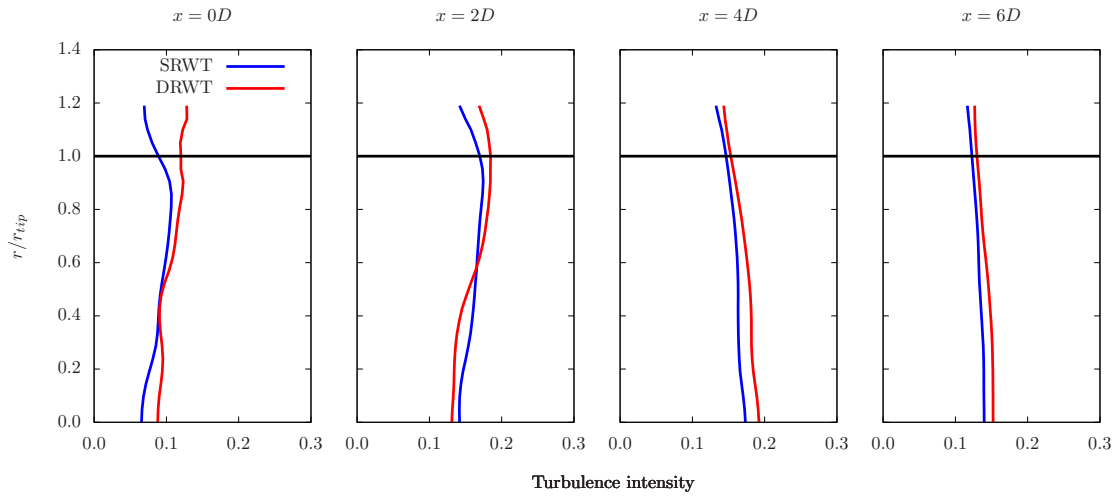

(a) Neutral

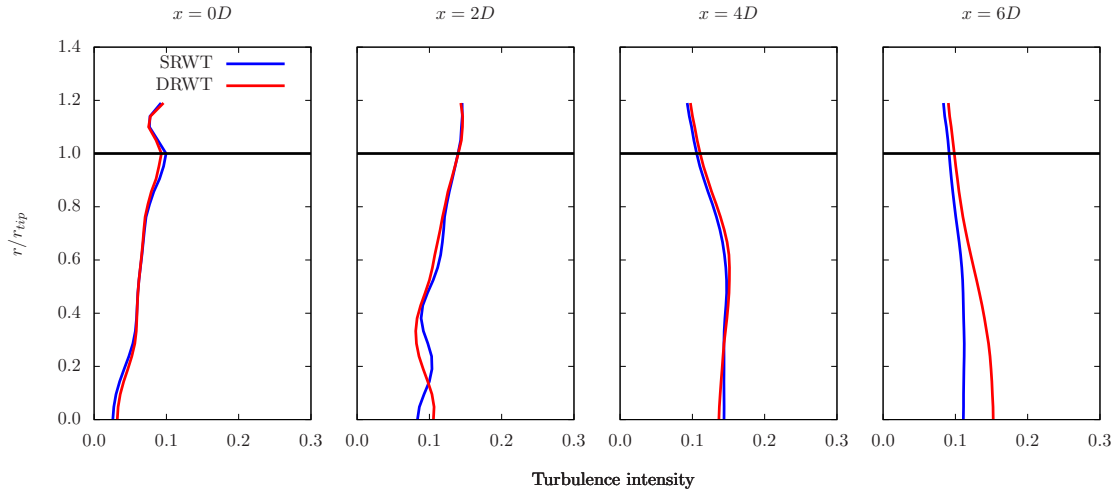

(b) Stable

Figure 9: Comparison between SRWT and DRWT of circumferentially averaged turbulence intensity at four downstream locations ($x/D = 0, 2, 4, \&6$) for (a) neutral, and (b) stable atmospheric conditions.

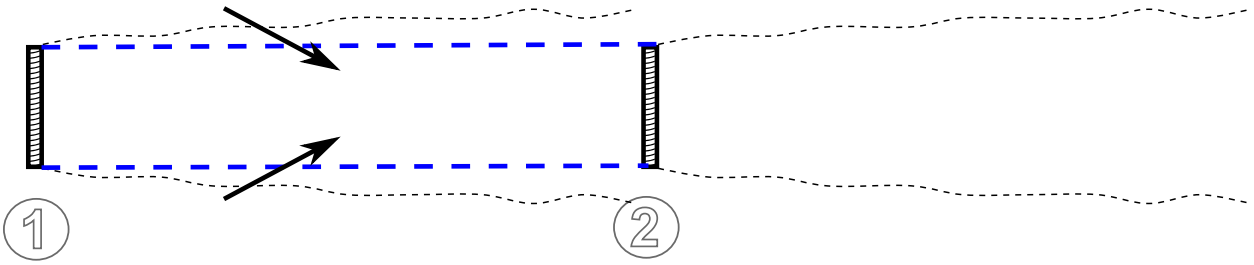

Figure 10: A schematic showing the cylindrical surface through which turbulent momentum flux is computed to quantify entrainment in turbine wake.

C. Aerodynamic Loads

Aerodynamic loads in terms of blade root bending moments are analyzed in this section. The approximations made to carry out this analysis should be re-emphasized: (1) the turbine is assumed to be infinitely rigid

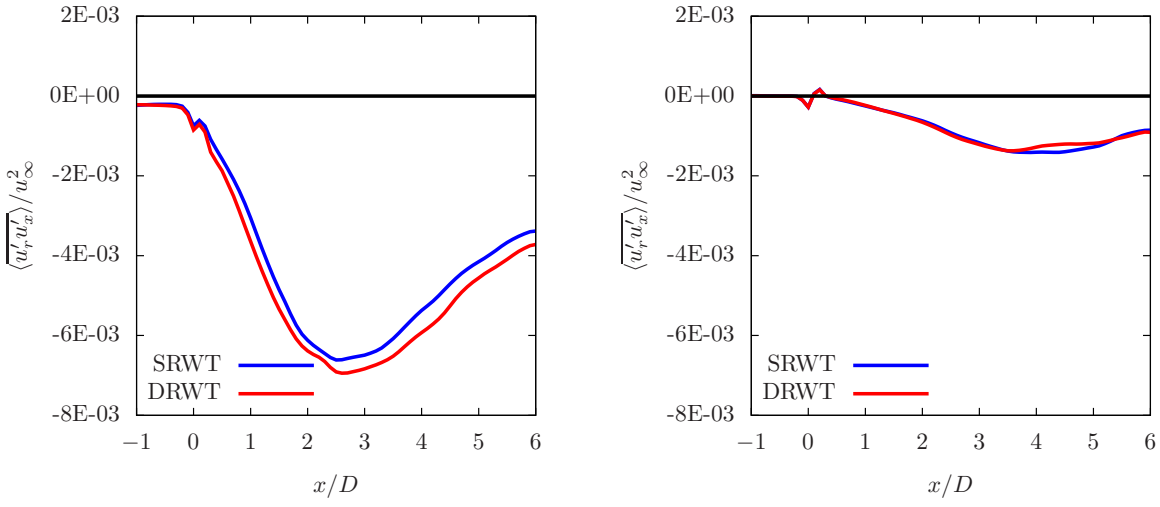

(a) Neutral

(b) Stable

Figure 11: Axial momentum entrainment due to turbulence.

(i.e., no deformation in turbine geometry is permitted), (2) the turbine is operated at a fixed rotation rate irrespective of the incoming wind speed (hence the tip speed ratio is fluctuating), and (3) the blade geometry is not resolved in the simulations and hence the potential interaction effects between the rotors are only approximately captured.

Figures 12 and 13 compare turbine power and out-of-plane (OOP) blade root bending moments in time and frequency domains. For the DRWT, turbine power is the sum of powers from the two rotor; blade root moment however is only plotted/compared for the main rotor unless otherwise stated. Figure 12 compares the DRWT and SRWT power and loads for the neutral ABL condition. The secondary rotor in the DRWT efficiently extracts power near the main rotor blade root region and hence the DRWT produces higher power than the SRWT throughout (see Fig. 12 (a)).

Fluctuations in power output are caused by: (a) azimuthal variation of incoming wind speed, and (b) inflow turbulence. Azimuthal variation of the mean wind speed in the atmospheric boundary layer translates into one per revolution variation for each blade of the turbine. Since the turbine blades are assumed to be identical, one-per-revolution excitation for each blade causes one-per-BPF excitation for the rotor, where BPF stands for blade passing frequency. Due to the ABL, deterministic power fluctuations at blade passing frequency and its harmonics are expected and are clearly observed in the results (see Fig. 12 (b)). In this figure the main rotor BPF is used to normalize frequency. Power fluctuations at secondary rotor BPF and harmonics are also present but they are much smaller in magnitude and are therefore inconspicuous in the figure.

A comparison of the OOP blade root bending moments in Fig. 12 (c and d) shows that both the mean and the fluctuating blade rotor bending moments are reduced for the main rotor of the DRWT. This is a very desirable feature of the DRWT - *increase in mean power and simultaneous reduction in main rotor blade root loads.*

Figure 13 compares the power and the OOP blade root moments for the stable ABL condition. Nothing much changes in comparison to the neutral case as far as power output is concerned - mean power is increased while fluctuating power stays approximately the same. The reduction in the OOP blade root moment by the DRWT however is much less in the stable ABL condition than in the neutral condition. Peaks in blade root moments (OOP) at the main rotor blade passing frequency and its harmonics suggest that the aerodynamic interaction between the main rotor and the secondary rotor has little impact on aerodynamic loads experienced by the main rotor.

We now investigate the loads on the secondary rotor. Figure 14 presents the power spectral densities of the secondary rotor OOP blade root moment for neutral and stable conditions. Contrasting the magnitudes in Figs. 14 and 12 & 13 elucidates that the mean and the fluctuating loads on the secondary rotor are in fact orders of magnitude smaller than those on the main rotor. Therefore, the secondary rotor can be designed

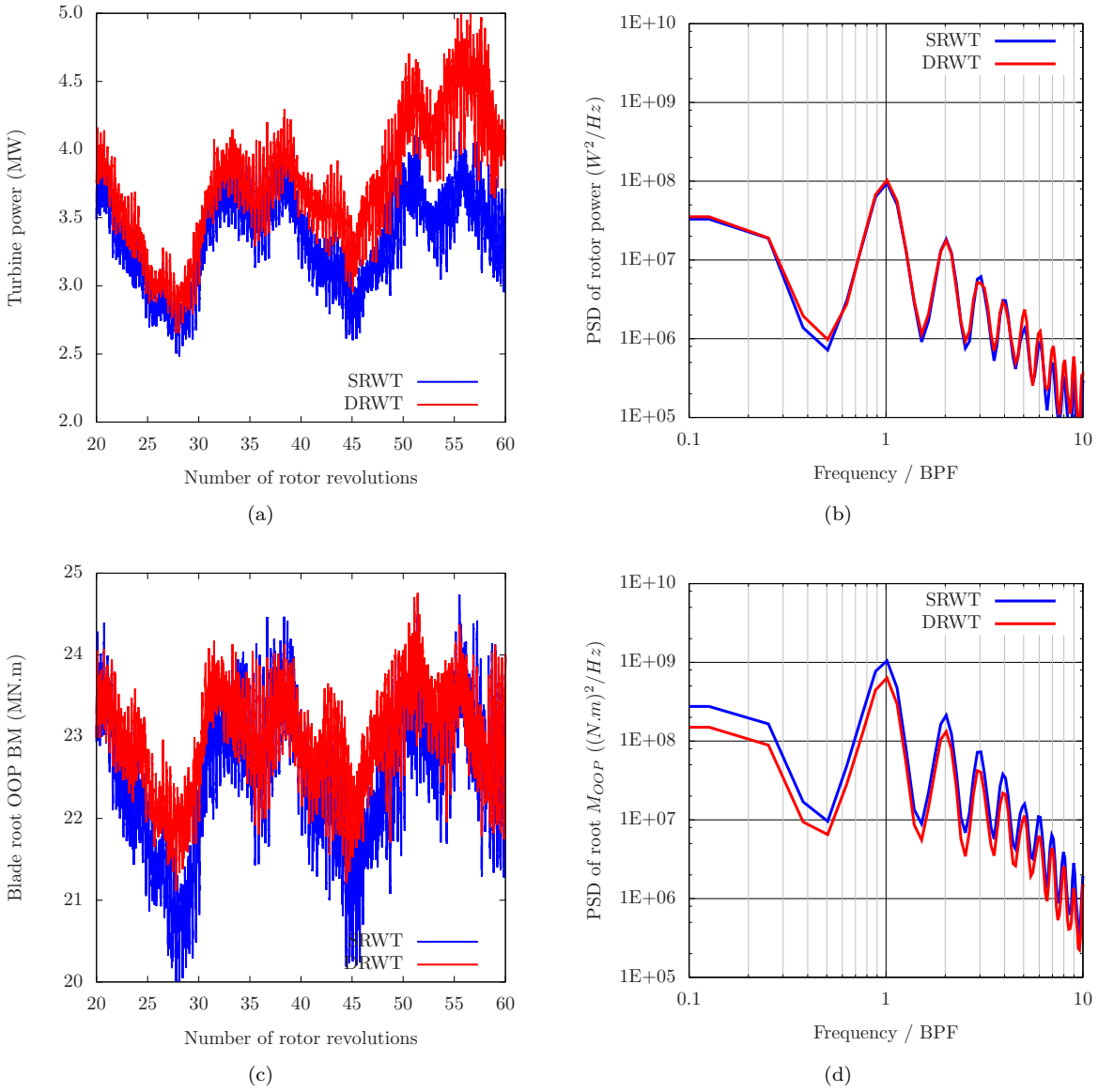

Figure 12: Neutral ABL simulation results

with relatively thin airfoils. The abscissa in Fig. 14 is normalized by the secondary rotor blade passing frequency. It can be seen that the peaks in the OOP blade root moment occur not just at the rotor BPF and its harmonics, but at many other frequencies. These are combination ("sum" and "difference") frequencies of the main and secondary rotors; aerodynamic noise at combination frequencies in dual-rotor propeller configurations have been studied elsewhere[30] by one of the authors. The mechanisms of noise generation at combination frequencies reported in Ref. 30 are exactly the same as what leads to the unsteady loads. In fact, noise generation is an indirect result of the unsteady loads on the rotor.

V. Conclusions

A numerical study is conducted using large eddy simulations to investigate the dual rotor wind turbine (DRWT) design proposed by Rosenberg *et al.*[1] The focus of the present study is to examine the aerodynamic performance and aerodynamic loads of a DRWT operating in (a) neutral and (b) stable atmospheric boundary layer conditions. The following conclusions are drawn from the results of this study.

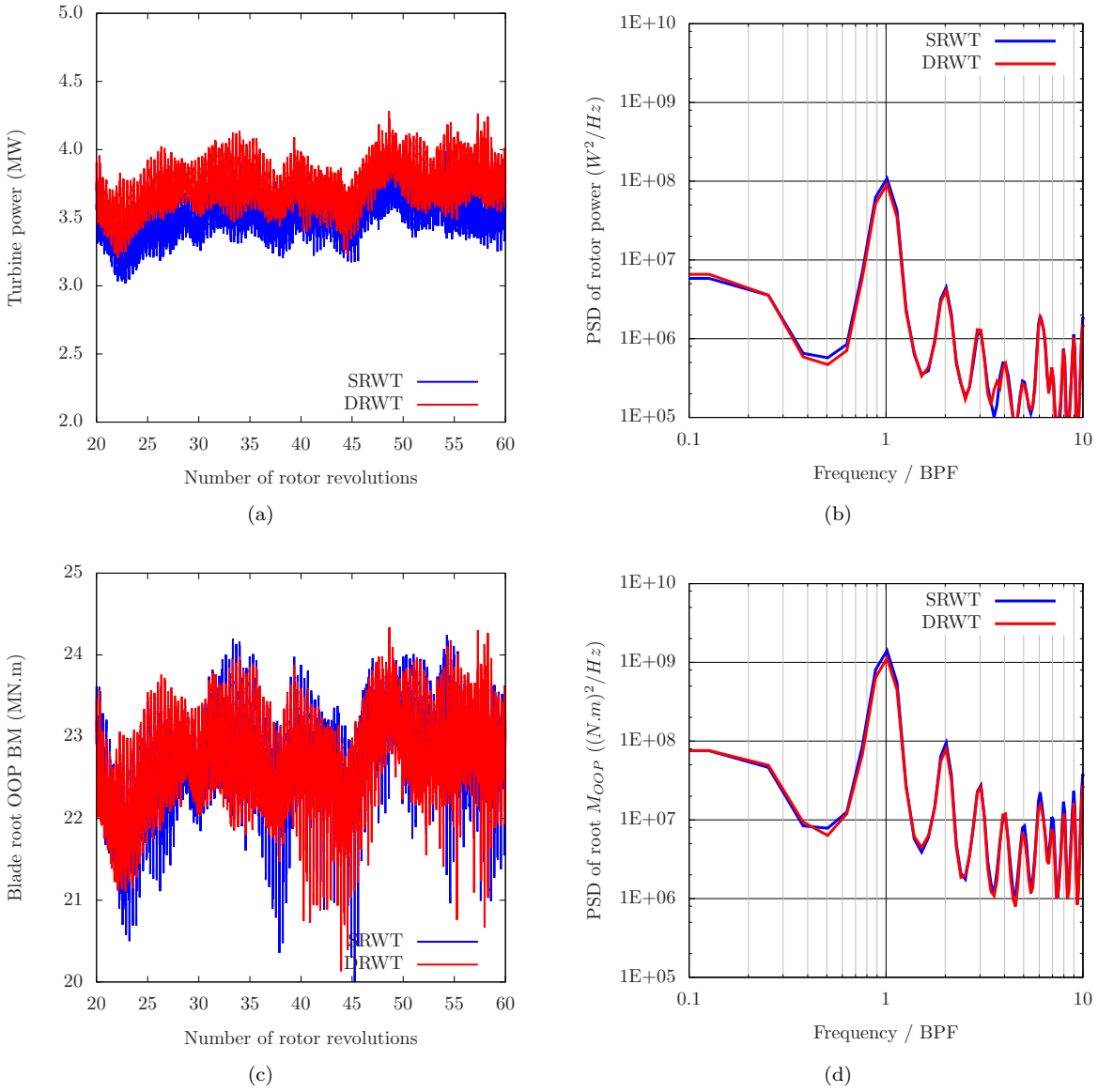

Figure 13: Stable ABL simulation results

1. The DRWT operating in isolation shows aerodynamic performance benefit for the two ABL conditions simulated. The performance benefit is due to increased capture of energy in the streamtube going through the blade root region.

2. The DRWT enhances wake mixing and entrainment of higher momentum fluid from outside the wake layer when the atmospheric (background) turbulence is moderately high (as in the neutral stability case simulated here).

3. The enhancement in wake mixing is associated with the increased turbulence intensity in the wake. This potentially has adverse consequences on fatigue loads on downstream turbines.

4. Spectral analysis of aerodynamic loads (measured as out-of-plane blade root moment and rotor power) shows slightly reduced levels of blade root bending moments for the main rotor in the DRWT. Harmonics of blade passing frequency are observed because of the azimuthal variation (due to the ABL) in the incoming wind speed.

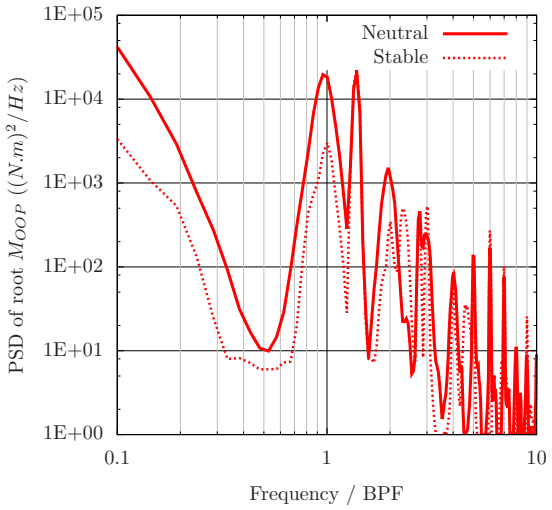

Figure 14: Secondary rotor simulation results

5. Spectral analysis of loads on the secondary rotor show peaks at "combination" (sum of BPFs of main and secondary rotors) frequencies.

VI. Acknowledgment

Funding for this work is provided by the National Science Foundation under grant number NSF/CBET-1438099 and the Iowa Energy Center under grant number 14-008-OG. The numerical simulations reported here are performed using the NSF XSEDE resources available to the authors under grant number TG-CTS130004.

References

[1]Rosenberg, A., Selvaraj, S., and Sharma, A., "A Novel Dual-Rotor Turbine for Increased Wind Energy Capture," *Journal of Physics: Conference Series*, Vol. 524, No. 1, 2014.

[2]Jung, S. N., No, T.-S., and Ryu, K.-W., "Aerodynamic performance prediction of a 30kW counter-rotating wind turbine system," *Renewable Energy*, Vol. 30, No. 5, 2005, pp. 631–644.

[3]Kanemoto, T. and Galal, A. M., "Development of intelligent wind turbine generator with tandem wind rotors and double rotational armatures (1st report, superior operation of tandem wind rotors)," *JSME International Journal Series B*, Vol. 49, No. 2, 2006, pp. 450–457.

[4]Kanemoto, T., "Wind turbine generator," Jan. 28 2010, US Patent App. 13/147,021.

[5]Selvaraj, S., *Numerical Investigation of Wind Turbine and Wind Farm Aerodynamics*, Thesis, Iowa State University, 2014.

[6]Jonkman, J., Butterfield, S., Musial, W., and Scott, G., "Definition of a 5-MW Reference Wind Turbine for Offshore System Development," 2009.

[7]Mikkelsen, R., *Actuator Disk Models Applied to Wind Turbines*, Thesis, Technical University of Denmark, 2003.

[8]Betz, A., *Schraubenpropeller mit Geringstem Energieverlust.*, Thesis, Gottingen Nachrichten, 1919.

[9]Goldstein, S., "On the vortex theory of screw propellers," *Proceedings of the Royal Society of London Series a-Containing Papers of a Mathematical and Physical Character*, Vol. 123, No. 792, 1929, pp. 440–465.

[10]Burton, T., Sharpe, D., Jenkins, N., and Bossanyi, E., *Wind Energy Handbook*, John Wiley & Sons Ltd., 2002.

[11]Ainslie, J. F., "Calculating the Flow Field in the Wake of Wind Turbines," *Journal of Wind Engineering and Industrial Aerodynamics*, Vol. 27, 1988, pp. 213–224.

[12]Snel, H., "Review of Aerodynamics for Wind Turbines," *Wind Energy*, Vol. 6, 2003, pp. 203–211.

[13]Vermeer, L. J., Srensen, J. N., and Crespo, A., "Wind Turbine Wake Aerodynamics," *Progress in Aerospace Sciences*, Vol. 39, 2003.

[14]Sanderse, B., Pijl, S. P. v. d., and Koren, B., "Review of Computational Fluids Dynamics for Wind Turbine Wake Aerodynamics," *Wind Energy*, 2011.

[15]Porté-Agel, F., Wu, Y., Lu, H., and Conzemius, R. J., "Large-Eddy Simulation of Atmospheric Boundary Layer Flow through Wind Turbines and Wind Farms," *Journal of Wind Engineering and Industrial Aerodynamics*, Vol. 99, 2011, pp. 154–168.

[16]Wu, Y. and Porté-Agel, F., "Large-Eddy Simulation of Wind-Turbine Wakes: Evaluation of Turbine Parametrisations," *Boundary-Layer Meteorology*, Vol. 138, No. 3, 2011.

[17]Jimenez, A., Crespo, A., Migoya, E., and Garcia, J., "Advances in Large-Eddy Simulation of a Wind Turbine Wake," *Journal of Physics: Conference Series*, Vol. 75, 2007.

[18]Jimenez, A., Crespo, A., Migoya, E., and J. Garica, J., "Large Eddy Simulation of Spectral Coherence in a Wind Turbine Wake," *Environmental Research Letters*, Vol. 3, 2008.

[19]Troldborg, N., Larsen, G. C., Madsen, H. A., Hansen, K. S., Srensen, J. N., and Mikkelsen, R., "Numerical simulations of wake interaction between two wind turbines at various inflow conditions," *Wind Energy*, Vol. 14, No. 7, 2011, pp. 859–876.

[20]Churchfield, M. J., Lee, S., Michalakes, J., and Moriarty, P. J., "A numerical study of the effects of atmospheric and wake turbulence on wind turbine dynamics," *Journal of Turbulence*, Vol. 13, No. 14, 2012, pp. 1–32.

[21]Churchfield, M., Lee, S., and Moriarty, P., "A Large-Eddy Simulation of Wind-Plant Aerodynamics," 2012.

[22]Smagorinsky, J., "General Circulation Experiments with the Primitive Equations I. The Basic Experiment," *Monthly Weather Review*, Vol. 91, 1963.

[23]Calaf, M., Meneveau, C., and Meyers, J., "Large eddy simulation study of fully developed wind-turbine array boundary layers," *Physics of Fluids*, Vol. 22, No. 1, 2010.

[24]Moeng, C., "A Large-Eddy-Simulation Model for the Study of Planetary Boundary-Layer Turbulence," *Journal of the Atmospheric Sciences*, Vol. 41, No. 13, 1984, pp. 2052???2062.

[25]Stull, R. B., *An Introduction to Boundary Layer Meteorology*, Kluwer Academic Publishers, 1988.

[26]Lee, S., Moriarty, P., and Churchfield, M., "On Fatigue Loadings of Wind Turbines from Atmospheric Boundary Layer," 2012.

[27]Jonkman, J. and Buhl, M., "FAST User's Guide," 2005.

[28]Witha, B., Steinfeld, G., and Heinemann, D., "High-resolution offshore wake simulations with the LES model PALM," *Wind Energy-Impact of Turbulence*, Springer, 2014, pp. 175–181.

[29]Newman, J. F. and Klein, P. M., "The impacts of atmospheric stability on the accuracy of wind speed extrapolation methods," *Resources*, Vol. 3, No. 1, 2014, pp. 81–105.

[30]Sharma, A. and Chen, H., "Prediction of Aerodynamic Tonal Noise from Open Rotors," *Journal of Sound and Vibration*, Vol. 332, No. 6, 2013.